Journal of Magnetism and Magnetic Materials 437 (2017) 29–41

Contents lists available at ScienceDirect

Journal of Magnetism and Magnetic Materials

journal homepage: www.elsevier.com/locate/jmmm

Research articles

# Regime of aggregate structures and magneto-rheological characteristics of a magnetic rod-like particle suspension: Monte Carlo and Brownian dynamics simulations

Kazuya Okada [a], Akira Satoh [b,*]

[a] School of Akita Prefectural University, Yurihonjo, Japan
[b] Department of Machine Intelligence and System Engineering, Akita Prefectural University, Yurihonjo, Japan

ARTICLE INFO

*Article history:*
Received 28 December 2016
Received in revised form 18 March 2017
Accepted 14 April 2017
Available online 21 April 2017

*Keywords:*
Magnetic colloidal dispersion
Monte Carlo
Brownian dynamics
Ferromagnetic rod-like particle
Regime change
Aggregate structure
Magneto-rheology
Viscosity

ABSTRACT

In the present study, we address a suspension composed ferromagnetic rod-like particles to elucidate a regime change in the aggregate structures and the magneto-rheological characteristics. Monte Carlo simulations have been employed for investigating the aggregate structures in thermodynamic equilibrium, and Brownian dynamics simulations for magneto-rheological features in a simple shear flow. The main results obtained here are summarized as follows. For the case of thermodynamic equilibrium, the rod-like particles aggregate to form thick chain-like clusters and the neighboring clusters incline in opposite directions. If the external magnetic field is increased, the thick chain-like clusters in the magnetic field direction grow thicker by adsorbing the neighboring clusters that incline in the opposite direction. Hence, a significant phase change in the particle aggregates is not induced by an increase in the magnetic field strength. For the case of a simple shear flow, even a weak shear flow induces a significant regime change from the thick chain-like clusters of thermodynamic equilibrium into wall-like aggregates composed of short raft-like clusters. A strong external magnetic field drastically changes these aggregates into wall-like aggregates composed of thick chain-like clusters rather than the short raft-like clusters. The internal structure of these aggregates is not strongly influenced by a shear flow, and the formation of the short raft-like clusters is maintained inside the aggregates. The main contribution to the net viscosity is the viscosity component due to magnetic particle-particle interaction forces in relation to the present volumetric fraction. Hence, a larger magnetic interaction strength and also a stronger external magnetic field give rise to a larger magneto-rheological effect. However, the dependence of the viscosity on these factors is governed in a complex manner by whether or not the wall-like aggregates are composed mainly of short raft-like clusters. An increase in the shear rate functions to simply decrease the effect of the magnetic particle-particle and the particle-field interactions.



## 1. Introduction

A suspension composed of magnetic fine particles smaller than micron-size has a recognised potential for application in a variety of engineering fields[1–5]. The specific application field for a magnetic particle suspension is usually dependent on an appropriate combination of both the geometrical and the magnetic characteristics of the particles. In the aspect of the geometrical shape, magnetic particles used for the synthesis of a magnetic suspension may typically exhibit spherical, rod-like, plate-like, disk-like and cube-like geometries. In the aspect of the magnetic properties, the characteristics of the particle magnetization are generally complex and consequently, for the purpose of analysis of the physical phenomena that are strongly dependent on the magnetic characteristics, several particle models have been developed.

These conventional modelling methods may be classified as a dipole model with a fixed magnetic moment [6–8] or with a changeable magnetic moment [9,10], a magnetic charge model [11–14] and a multi-dipole model [4,15,16]. The multi-dipole model is often suitable as a magnetization model for magnetic particles with a complex geometrical shape. The physical behaviour of a magnetic suspension in a flow field and an external magnetic field is generally more complex for the case of dispersed particles with a complex shape or magnetic characteristics. In order to accomplish a successful application of these suspensions in the commercial field, the analysis and development of an accurate

* Corresponding author.
*E-mail address:* asatoh@akita-pu.ac.jp (A. Satoh).

http://dx.doi.org/10.1016/j.jmmm.2017.04.034
0304-8853/

control of the physical characteristics is considered to be indispensable.

Typical application areas of magnetic particle suspensions are the fields of magnetic recording material engineering [4], fluid engineering [1–3], biomedical engineering [5] and environmental resource engineering [17–19]. In the field of magnetic recording material engineering, magnetic particle suspensions are treated as an intermediary medium to obtain the final goal of recording materials. An example of a control technique for obtaining a successful application may be to control the growth of the crystal structure of the magnetic material by means of an external magnetic field. The primary applications in the field of fluid engineering are mechanical dampers and actuators [2,3]. These applications require magnetic suspensions with a large magneto-rheological characteristic whilst their fluid characteristics have to be controlled in a desirable manner to exhibit suitable properties by means of an applied magnetic field and a flow field. Magnetic colloidal dispersions, known as ferrofluids, may be used for controlling the process of heat transfer [20,21] where a sophisticated cooling technique is indispensable in the engineering fields of microelectronic devices and nuclear reactors. The kind of studies relating to the development of controlling the heat transfer in the engineering applications have recently been expanded to the application of new functional nanofluids [22–25]. In the field of biomedical engineering, it is hopeful that the application of magnetic suspensions may facilitate a magnetically targeted drug delivery system [5,26,27] and magnetic particle hyperthermia [28–31]. There are also challenging technological applications to be found in environmental resource engineering for the recovery of specific substances such as hazardous heavy metal molecules found in environmental waste and pollutants and the extraction of valuable noble metal molecules from water, i.e. from seas, lake, etc., [23–25].

In the present study we focus on the application field of fluid engineering. Mechanical dampers and actuators require suspensions with a large magneto-rheological effect that is controlled using an external magnetic field together with a sophisticated mechanical design incorporating a fluid reservoir and orifice. In the pioneering days of magnetic fluids or ferrofluids, a variety of studies had been conducted from the viewpoint of their application to mechanical dampers and actuators [1]. However, ferrofluids composed of nano-sized spherical magnetic particles in a base liquid cannot exhibit a sufficiently strong magneto-rheological effect and so a successful application regarding mechanical dampers and actuators is unlikely, although the design of a mechanical seal using a ferrofluid is an example of a successful commercial application [32–34]. The current trends regarding ferrofluids are described in the Ref. [35], which includes studies in regard to phase behaviour and polydispersity. Hence, in order to develop devices making use of magneto-rheological characteristics, we are required to synthesize suspensions that exhibit a sufficiently large magneto-rheological characteristic that is able to provide a practical function in a commercial product. Since it is known that non-spherical magnetic particles under certain conditions will offer a large resistance to the ambient flow[36–38], rod-like, disk-like and cube-like particles may be hopeful magnetic particle geometries for synthesizing magneto-rheological suspensions.

Modern synthesis technologies enable one to generate magnetic particles with a variety of shapes and magnetic properties such as rod-like [39–43], disk-like [44,45] and cube-like particles [46–51]. Different from the conventional synthesis technologies, where a new magnetic characteristic is generated by altering the composition of the constituting materials (molecules), the new generation of fine particles is made by design in order to obtain the most desirable properties as functional particles [52,53]. The concept of this development approach corresponds to particular kinds of design engineering with regard to mechanical machines and such non-spherical particle suspensions have actively been studied from various points of view. Dynamic behaviours such as particle orientation and tumbling motion in magnetic rod-like particle suspensions have been investigated by particle-based simulations [6,7,12,54,55]. Features such as yield stress in these suspensions may be strongly dependent on aggregation factors such as the formation and orientation of linear chain-like clusters [56,57]. Moreover, the internal structure of aggregates may undergo a regime change in the particle aggregation due to a dependency on the magnetic field strength and magnetic particle-particle interaction strength [58]. The geometrical shape of non-spherical particles has a significant influence on the magneto-rheological characteristics [59–61] since, for example, rod-like particles offer a much larger resistance to the ambient flow than spherical particles, resulting from the magnetic particle-particle interactions and a restriction of their orientation to the magnetic field direction. If a dilute suspension of magnetic rod-like particles is addressed, certain assumptions may be made for which theoretical approaches are feasible for investigating the rheological characteristics [36,38,62,63].

In contrast to ferromagnetic particles, spindle-like haematite particles are magnetized in a direction normal to the particle axis direction, exhibit much weaker magnetization than the magnetite [41–43,64,65] and give rise to quite different properties. For instance, suspensions composed of spindle-like haematite particles were theoretically predicted to exhibit a negative viscosity under certain conditions of an applied magnetic field [66–69], and this has been experimentally verified using a cone-plate-type rheometer [70]. The aggregate structures of rod-like haematite particles have been investigated by molecular simulations for the case of a non-equilibrium thermodynamic state [71].

There are a variety of studies regarding suspensions of disk-like and cube-like particles by means of both theoretical and experimental approaches. For the case of magnetic disk-like particles, orientational characteristics and aggregate structures have been investigated [72,73] and also the dependence of the magneto-rheological characteristics on a variety factors, including the aggregate structures, has been elucidated [59,74–76]. The sedimentation characteristics of magnetic plate-like particles in the gravitational field are found to be strongly dependent on their orientational properties [77]. Cube-like particles are not an axisymmetric particle but are the next simpler model for theoretical analyses or simulations. Recently, therefore, the microstructure of mono-layers and multi-layers of cube-like particles on a material surface has actively been elucidated experimentally and theoretically [78–82] although currently the rheological characteristics of both cube-like and disk-like particles have not been sufficiently investigated [76,83].

As already pointed out, we here concentrate on suspensions composed of magnetic particles from a fluid engineering point of view and address suspensions composed of ferromagnetic rod-like particles. These particles are typically magnetized in the particle axis direction and exhibit a large magneto-rheological effect [36,38,63], which is in contrast to rod-like haematite particle suspensions where a negative magnetic rheological effect may arise for particular conditions of an external magnetic field [66–70]. As already mentioned, specialised magnetic particles are generated by design in order to obtain the most desirable characteristics as functional particles [52,53], therefore it may be valuable to elucidate the rheological features of a suspension of rod-like particles exhibiting various kinds of magnetic characteristics. From this background, in a previous study [58], we treated a suspension composed of magnetic rod-like particles that are modelled as a spherocylinder with a magnetic dipole moment at the particle centre orientated in the particle axis direction. In that study, we

investigated the characteristics of a phase change in the aggregate structures, that is dependent on a variety of factors, for a system in thermodynamic equilibrium.

In the present study, we address the type of ferromagnetic rod-like particles that may be modelled as a spherocylinder dipole with a plus and a minus magnetic charge at the centre of each hemisphere cap. We here attempt to elucidate the conditions for regime change in the aggregate structures and their relationship to the magneto-rheological effect for various situations of the external magnetic field strength and a shear flow. Here, characteristics of the phase change are investigated by Monte Carlo (MC) simulations in thermodynamic equilibrium, and the magneto-rheological properties are investigated in a simple shear flow by Brownian dynamics (BD) simulations. From the former simulations, we attempt to clarify the dependencies relating to the aggregate structures, and from the later simulations, the dependencies relating to the magneto-rheological effect by considering factors such as the magnetic particle-particle interaction strength and the external magnetic field strength. As in the previous study [58], attention will be given to the observation of a regime change in the aggregate structures for various cases of the above-mentioned factors and the effect of the shear rate of a simple shear flow. In order to investigate the magneto-rheological effect in detail, the net viscosity is decomposed into three viscosity components, which arise from the torque due to the magnetic particle-field interaction together with the torque and the force due to the interaction between particles.

## 2. Particle model

We here employ the model of a magnetic spherocylinder to represent a ferromagnetic rod-like particle, as shown in Fig. 1. The spherocylinder has a magnetic charge of $+q$ and $-q$ at the centre of each hemisphere cap, where the length of the cylinder body is denoted by $l_0$, the diameter of the hemispherical cap by $d$, and the total length of the spherocylinder by $l = l_0 + d$. In a particle suspension, a particle is typically coated with a steric layer or an electric double layer in order to maintain stability, hence, the particle is assumed to be covered by a uniform steric layer with thickness $\delta$ [84,85]. In MC simulations, a particle suspension is assumed to be in thermodynamic equilibrium and so is suitable for investigating the aggregate structure, whilst in BD simulations, the suspension may be subject to a simple shear flow $\boldsymbol{U} = (\dot{\gamma}y, 0, 0)$ with shear rate $\dot{\gamma}$ and so is suitable for elucidating the magneto-rheological characteristics. In both MC and BD simulations, an external magnetic field is applied in the $y$-axis direction as $\boldsymbol{H} = (0, H, 0)$.

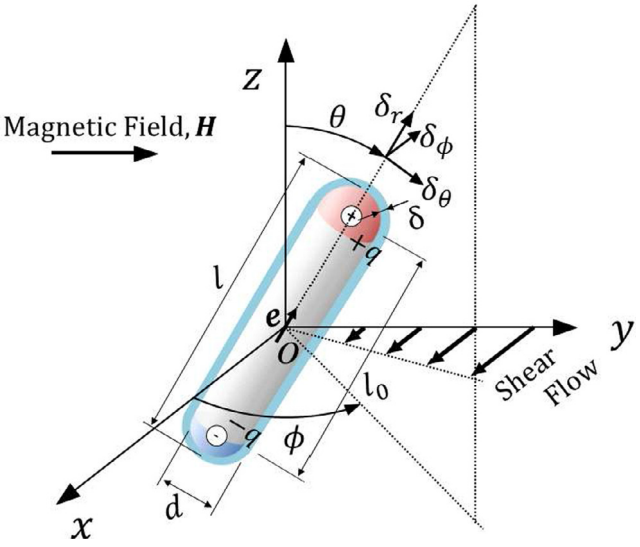


**Fig. 1.** Particle model.

In performing MC simulations, the particle-particle and particle-field interactions are required to be written as mathematical expressions. If the position vector of the centre of particle $i$ is denoted by $\boldsymbol{r}_i$ and the particle direction by $\boldsymbol{e}_i$, then the magnetic interaction energy between particles $i$ and $j$, $u_{ij}^{(m)}$, and the magnetic particle-field interaction energy, $u_i^{(H)}$, are expressed, as [84,85]

$$u_{ij}^{(m)} = kT\lambda\left\{\frac{1}{\left|\mathbf{r}_{ij}+\frac{l_0}{2}(\mathbf{e}_i-\mathbf{e}_j)\right|}-\frac{1}{\left|\mathbf{r}_{ij}+\frac{l_0}{2}(\mathbf{e}_i+\mathbf{e}_j)\right|}-\frac{1}{\left|\mathbf{r}_{ij}-\frac{l_0}{2}(\mathbf{e}_i+\mathbf{e}_j)\right|}+\frac{1}{\left|\mathbf{r}_{ij}-\frac{l_0}{2}(\mathbf{e}_i-\mathbf{e}_j)\right|}\right\} \tag{1}$$

$$u_i^{(H)} = -kT\xi\ \boldsymbol{e}_i\cdot\boldsymbol{H}/H \tag{2}$$

in which $k$ is Boltzmann's constant, $T$ is the absolute temperature of the based liquid, and $\boldsymbol{r}_{ij} = \boldsymbol{r}_i - \boldsymbol{r}_j$ is the relative position vector from particle $j$. The non-dimensional parameters $\lambda$ and $\xi$ imply that the strengths of magnetic particle-particle and magnetic particle-field interactions, expressed as $\lambda = \mu_0(ql_0)^2/(4\pi d^3kT)$ and $\xi = \mu_0 mH/(kT)$, respectively, where $\mu_0$ is the permeability of free space, and $m$ is the magnitude of the magnetic moment $\boldsymbol{m}_i = ql_0\boldsymbol{e}_i$.

The particle is assumed to be covered by a uniform steric layer, which induces a repulsive interaction between the particles when the steric layers overlap. However, it is difficult to express this interaction energy as a single mathematical expression for the overlap of two spherocylinder particles. Therefore, as in the previous study [69], the spherocylinder particle is modelled as a linear sphere-connected particle with each sphere covered by a steric layer, and the repulsive interaction energy $u_{ij}^{(V)}$ is evaluated by calculating and summing the energies for all the pairs of spherical particles belonging to the two different spherocylinder particles. In this calculation, we employ the well-known expression for the overlap of the steric layers covering two equal-sized spheres [1]. The strength of the repulsive interaction energy due to the overlap is characterized by the non-dimensional parameter $\lambda_V = n_s kT/2$, where $n_s$ is the number of surfactant molecules per unit area on the surface of the spherical particles [84,85]. In the MC approach, the above-mentioned interactions are sufficient for conducting the simulation for the purpose of analyzing the internal structure of aggregates.

In BD simulations, particle forces and torques rather than the interaction energies are required to be calculated every time step for advancing the simulation procedure. We straightforwardly obtain the expressions for the magnetic force $\boldsymbol{F}_{ij}^{(m)}$ and torque $\boldsymbol{T}_{ij}^{(m)}$ acting on particle $i$ by particle $j$, the force $\boldsymbol{F}_{ij}^{(V)}$ and torque $\boldsymbol{T}_{ij}^{(V)}$ due to the overlap of the steric layers, and the magnetic torque $\boldsymbol{T}_i^{(H)}$ due to the interaction between the magnetic moment and an applied magnetic field. These expressions have already been shown in the Refs. [84,85], and therefore we do not exhibit them in the present paper.

## 3. Monte Carlo method

MC simulations have been employed for investigating the aggregate structures of particles in thermodynamic equilibrium, i.e., there is no shear flow. In the case of a strongly-interacting system, the conventional Metropolis MC method [86] cannot capture physically reasonable aggregate structures from the dispersed particles. This is mainly because the constituent particles forming a cluster cannot dissociate from the cluster to join in a growing

cluster, which implies that the convergence to an equilibrium state is extraordinary slow with conventional MC simulations. In the cluster-moving MC method [84,85], the clusters which are formed during the process of the simulation are moved as unitary particles, which gives rise to physically reasonable aggregate structures, even in a strongly-interacting system such as the present magnetic particle system. The assessment regarding the acceptance or rejection of a new position or a new orientation of a cluster of interest is conducted according to the usual Metropolis method. The combination of cluster-moving steps with the conventional particle-based steps gives rise to the formation of physically reasonable aggregate structures within an acceptable computation time. If the movement and orientation of the clusters are not frequently attempted in relation to the single particle steps, any particles without attractive forces which become accidentally located in the range of a cluster may quite easily drift away again with advancing simulation steps. Therefore, it is understood that the cluster-moving Monte Carlo method is a powerful simulation tool for analyzing the microstructure of the present system of magnetic rod-like particles where large clusters are expected to be formed in certain conditions. Referring to the previous study [87], in the present simulations we have attempted to analyze the cluster formation and then to move these clusters every 20 MC steps.

The main part of the cluster-moving algorithm, that is, the transition from microscopic state $i$ to state $j$, is written as

a. Check the formation of clusters
b. Select a cluster
c. Compute the interaction energy of the selected cluster with the other clusters, $U$
d. Move the cluster randomly and compute the interaction energy of the cluster at the new position, $U'$
e. If $\Delta U = U' - U \leqslant 0$, then accept the new position and return to step b
f. If $\Delta U > 0$, then generate a uniform random number $R$ $(0 < R < 1)$
   f.1. If $\exp(-\Delta U/kT) \geqslant R$, then accept the new position and return to step b
   f.2. If $\exp(-\Delta U/kT) < R$, then reject the movement, retain the old position, and return to step b (the old state is regarded as a new state for averaging procedures)

In this algorithm, the interaction energy $U$ is evaluated by summing the magnetic particle-particle interaction energy, $u_{ij}^{(m)}$, the magnetic particle-field interaction energy, $u_i^{(H)}$, and the repulsive interaction energy, $u_{ij}^{(V)}$. It is noted that the procedures (e) and (f) in the above algorithm are the conventional Metropolis MC method [86].

Finally, it should be noted that the Monte Carlo method is a fully established simulation technique, and therefore simulation results obtained by this method are generally accepted to be sufficiently reliable. In certain situations, Monte Carlo results may be regarded as an exact solution, although the accuracy of the solution is dependent on the appropriate modelling of the interaction potentials between dispersed particles (or molecules in a molecular system).

## 4. Brownian dynamics method

BD simulations have been adopted for elucidating the magneto-rheological characteristics of the present suspension by analyzing the behaviour of the magnetic rod-like particles in a simple shear flow. Since the detailed expressions have already been shown in other articles [76,71], we here summarize only a few important expressions for performing the present BD simulations. The simulated rod-like particles move with translational and rotational Brownian motion in a simple shear flow $\boldsymbol{U}$ that is characterized by the angular velocity vector $\boldsymbol{\Omega}$ and the rate-of-strain tensor $\boldsymbol{E}$. In the case of the axisymmetric particle, the equation of motion can be decomposed into the translational motion in the particle axis direction (denoted by subscript $\parallel$) and the translational motion in the direction normal to the particle axis (denoted by subscript $\perp$). The equation of translational motion is expressed as [76,71]

$$\boldsymbol{r}_{\parallel}(t+\Delta t) = \boldsymbol{r}_{\parallel}(t) + \boldsymbol{U}_{\parallel}\Delta t + \frac{1}{kT} D_{\parallel}^{T} \boldsymbol{F}_{\parallel}^{p}(t)\Delta t + \Delta r_{\parallel}^{B}\boldsymbol{e}(t) \tag{3}$$

$$\boldsymbol{r}_{\perp}(t+\Delta t) = \boldsymbol{r}_{\perp}(t) + \boldsymbol{U}_{\perp}\Delta t + \frac{1}{kT} D_{\perp}^{T} \boldsymbol{F}_{\perp}^{p}(t)\Delta t + \Delta r_{\perp 1}^{B}\boldsymbol{e}_{\perp 1}(t) + \Delta r_{\perp 2}^{B}\boldsymbol{e}_{\perp 2}(t) \tag{4}$$

From the equation of motion of the rotational motion, the equation providing the particle direction $\boldsymbol{e}$ is obtained as [76,71]

$$\boldsymbol{e}(t+\Delta t) = \boldsymbol{e}(t) + \boldsymbol{\Omega}_{\perp} \times \boldsymbol{e}\ \Delta t + \frac{1}{kT} D_{\perp}^{R} \boldsymbol{T}_{\perp}^{p}(t) \times \boldsymbol{e}\Delta t - \frac{Y^{H}}{Y^{C}}((\boldsymbol{\varepsilon}\cdot\boldsymbol{e}\boldsymbol{e}) : \boldsymbol{E}) \times \boldsymbol{e}\Delta t + \Delta\phi_{\perp 1}^{B}\boldsymbol{e}_{\perp 1}(t) + \Delta\phi_{\perp 2}^{B}\boldsymbol{e}_{\perp 2}(t) \tag{5}$$

In these equations, $D^T$ and $D^R$ are the diffusion coefficients of the spherocylinder particles for the translational and rotational motion, $Y^C$ and $Y^H$ are the resistance functions, $\boldsymbol{e}_{\perp 1}$ and $\boldsymbol{e}_{\perp 2}$ are the unit vectors normal to each other in the plane normal to the particle axis, $\Delta t$ is the time interval, and $\boldsymbol{\varepsilon}$ is the third-rank tensor called Eddington's epsilon. Moreover, $\Delta r_{\parallel}^{B}$, $\Delta r_{\perp 1}^{B}$ and $\Delta r_{\perp 2}^{B}$ are the random displacements inducing the translational Brownian motion, and $\Delta\phi_{\perp 1}^{B}$ and $\Delta\phi_{\perp 2}^{B}$ are the random displacements inducing the rotational Brownian motion. The random displacements have the following stochastic characteristics:

$$\langle \Delta r_{\parallel}^{B}\rangle = \langle \Delta r_{\perp 1}^{B}\rangle = \langle \Delta r_{\perp 2}^{B}\rangle = 0, \quad \langle (\Delta r_{\parallel}^{B})^{2}\rangle = 2D_{\parallel}^{T}\Delta t,$$
$$\langle (\Delta r_{\perp 1}^{B})^{2}\rangle = \langle (\Delta r_{\perp 2}^{B})^{2}\rangle = 2D_{\perp}^{T}\Delta t \tag{6}$$

$$\langle \Delta\phi_{\perp 1}^{B}\rangle = \langle \Delta\phi_{\perp 2}^{B}\rangle = 0, \quad \langle (\Delta\phi_{\perp 1}^{B})^{2}\rangle = \langle (\Delta\phi_{\perp 2}^{B})^{2}\rangle = 2D_{\perp}^{R}\Delta t \tag{7}$$

As shown in Fig. 1, the particle axis direction $\boldsymbol{e}$ is expressed as a zenithal angle $\theta$ from the $z$-axis and an azimuthal angle $\phi$ from the $x$-axis. Moreover, the above unit vectors $(\boldsymbol{e}_{\perp 1}, \boldsymbol{e}_{\perp 2})$ are assumed to be $(\boldsymbol{\delta}_{\theta}, \boldsymbol{\delta}_{\phi})$.

In BD simulations, it is seen that the present phenomenon is characterized by the four non-dimensional parameters $\lambda = \mu_0(ql_0)^2/(4\pi d^3 kT)$, $\lambda_V = n_s d^2 kT/2$, $\xi = \mu_0 mH/(kT)$ and $Pe = \dot{\gamma}/(3D_{\perp}^{R})$, where $Pe$ is the Peclet number and implies the strength of the influence of the viscous shear force relative to that of the rotational Brownian motion. In this study, the expressions for the diffusion coefficients of a cylinder particle with diameter $d$ and length $l$ are employed, and these expressions are shown in Ref. [85].

We here discuss the characteristics of the magneto-rheological effect at a deeper level by decomposing the net viscosity $\eta_{yx}^{M}$ into the three factors, expressed as $\eta_{yx}^{M}$ $(=\eta^{total})=\eta_{yx}^{F} + \eta_{yx}^{TH} + \eta_{yx}^{FT}$. These components imply that $\eta_{yx}^{TH}$ is the viscosity component due to the torque resulting from the magnetic particle-field interaction, and $\eta_{yx}^{F}$ and $\eta_{yx}^{FT}$ are the viscosity components due to the force and the torque arising from the particle-particle interactions, respectively [69]. It is noted that the results of the viscosities, shown later, are dimensionless quantities that were obtained by dividing the data by the volumetric fraction $\phi_V$ and the viscosity $\eta_s$ of a base liquid [36,38,63].

Finally, it should be noted that the present Brownian dynamics approach enables us to discuss the characteristics of the viscosity

components separately, which has a great advantage compared with an experimental approach, whereby such a detailed analysis regarding the viscosity components would be significantly difficult.

## 5. Parameters for simulations

Unless specifically noted, the present results were obtained by adopting the following values. The volumetric fraction of magnetic rod-like particles is $\phi_V = 0.05$, the number of particles $N = 512$, the thickness of the steric layer $\delta^*$ ($=\delta/d$) = 0.15, the repulsive interaction $\lambda_V = 150$, the particle aspect ratio $r_p$ ($=l/d$) = 5, the cutoff radius for calculating particle-particle interactions $r_{coff}^*$ ($=r_{coff}/d$) = $5r_p$, and the Peclet number $Pe = 1$. Moreover, the non-dimensional parameters $\lambda$, $\xi$ and $Pe$ are addressed in a wide range of values with $\lambda$ = 10–50, $\xi$ = 0.1–20 and $Pe$ = 1–20. In the MC simulations, the total MC steps are taken as $N_{timemx}$ = 1,000,000, and the last 80% of data were used for the averaging procedure. In the BD simulations, the total number of time steps per simulation run is $N_{timemx}$ = 5,000,000 and the last 50% of data were used for the averaging procedure. We employed the common periodic boundary condition in all the axis directions to treat the boundary surfaces of the simulation box for the case of MC simulations. In the BD simulations, we employed the Lees-Edwards boundary condition [86] that is useful for molecular simulations of a system in a flow field. A magnetic field and a simple shear flow are applied in the $y$- and $x$-axis direction, respectively. The spherocylinder particles are expected to aggregate in the magnetic field direction ($y$-axis direction) because they are magnetized in the particle axis direction. Hence, we employed a rectangular-parallelepiped simulation box in the field direction with a square base. The size of the simulation box ($L_x$, $L_y$, $L_z$) is set as $L_y = 2L_x$ and $L_x = L_z$. An initial position of particles is randomly set using quasi-random numbers, and an initial orientation of particles is assigned in such a way that the magnetic moment of each particle aligns in the magnetic field direction. From preliminary simulations, we employed a time interval $\Delta t^*$ as $\Delta t = 0.00002$. It is noted that for a case of $Pe \gg 1$, $\lambda \gg 1$ and $\xi \gg 1$, the effect of either one is more dominant than the effect of Brownian motion.

## 6. Order parameter

In the Monte Carlo simulation, for evaluating the order of the whole system, we focus on the order parameter $S^{(e)}$ of the particle directions and $S_{ey}$ of the alignment of the magnetic moments with the magnetic field direction that are expressed, respectively, as

$$S^{(e)} = \frac{1}{N_{pair}} \left\langle \sum_{i=1}^{N} \sum_{\substack{j=1 \\ (j>i)}}^{N} P_2(\cos \psi_{ij}^{(p)}) \right\rangle \tag{8}$$

$$S_{ey} = \frac{1}{N} \langle \sum_{i=1}^{N} P_2(\cos \theta_i^{(m)}) \rangle \tag{9}$$

in which $P_2(-)$ is a second Legendre polynomials, expressed as $P_2(\cos \psi_{ij}^{(p)}) = (\cos^2 \psi_{ij}^{(p)} - 1)/2$, where $\psi_{ij}^{(p)}$ is an angle between the orientation of the particle directions for particles $i$ and $j$. Also, $\theta_i^{(m)}$ is an angle between the particle direction of particle $i$ and the magnetic field direction. $N_{pair}$ is the number of all pairs of particles, expressed as $N_{pair} = N(N-1)/2$, and $\langle - \rangle$ is the ensemble average.

## 7. Results and discussion for thermodynamic equilibrium

### 7.1. For the case of almost no applied magnetic field

Fig. 2(a) and (b) show results of the aggregate structures for the case of almost no applied magnetic field $\xi = 0.1$: Fig. 2(a) and (b) show snapshots for $\lambda = 20$ and 30, respectively. It is noted that a snapshot on the right-hand side in each case is viewed from a different direction to observe the aggregates in the main snapshot on the left-hand side more clearly. Fig. 3 shows results of the order parameter $S^{(e)}$ defined in Eq. (8): it is noted that the value of the order parameter will increase as the constituent particles of clusters incline more significantly in the same direction.

For the case of $\lambda = 20$, shown in Fig. 2(a), short raft-like and chain-like clusters composed of two or three particles are observed to be formed, and these clusters and particles tend to form a large and loosely-packed aggregate. However, since the magnetic interaction is not sufficiently strong for a large stable cluster formation, this loose aggregate is not formed in the case of strong interaction forces between particles. Moreover, they do not show a particular directional characteristic but seem to incline randomly in any direction. These features are verified by an almost zero value of the order parameter at $\lambda = 20$ for $\xi = 0.1$ in Fig. 3. For the case of $\lambda = 30$, shown in Fig. 2(b), the rod-like particles aggregate to form thick chain-like clusters, and the neighboring clusters incline in opposite directions to each other, which leads to a lower magnetic interaction energy of the system when there is almost no applied magnetic field. These linear chain-like clusters are formed by neighboring particles in a cluster by locating with the magnetic charge of one particle being in contact with the opposite magnetic charge of the other particle. The number of the clusters that align in a particular direction is almost equal to that of the clusters inclining in the opposite direction with the condition of almost zero magnetic field $\xi = 0.1$. Also, it is seen that these clusters are arranged in a wall-like formation rather than randomly arranged and this configuration is expected to give rise to a lower total interaction energy of the system.

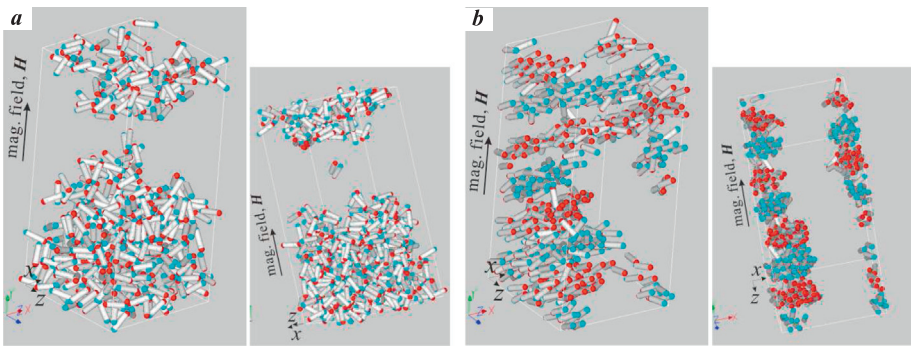


**Fig. 2.** Aggregate structures for (a) $\lambda = 20$ and (b) $\lambda = 30$ in the situation of almost zero magnetic field $\xi = 0.1$: the snapshot on the right-hand side of each figure is a different angle view for observing the aggregate structures more clearly.

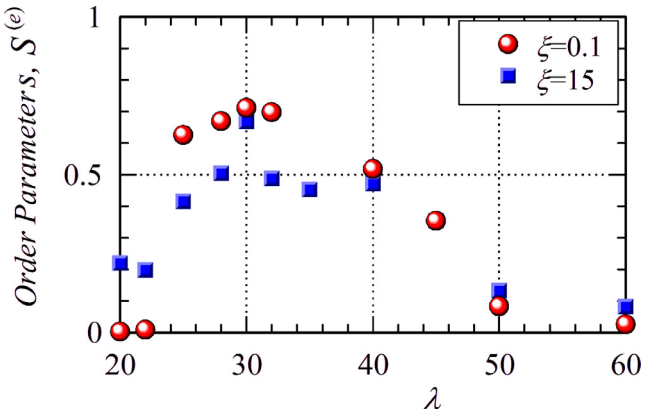


**Fig. 3.** Order parameter of particle directions as a function of the magnetic interaction strength.

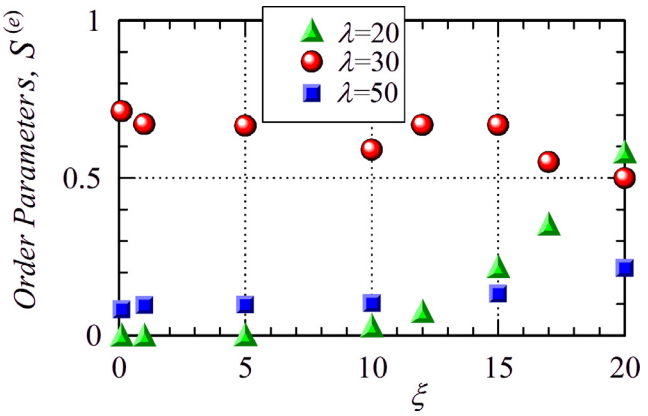


**Fig. 5.** Order parameter of particle directions as a function of the magnetic field strength.

Fig. 3 shows that the order parameter exhibits a significant peak value of $S^{(e)} \simeq 0.7$ at $\lambda = 30$, which is due to the constituent particles of a thick chain-like cluster tending to incline towards the same direction. In the range of $\lambda \gtrsim 30$, the order parameter gradually decreases to almost zero at $\lambda = 60$ with increasing magnetic interaction strength. It should be noted that this characteristic is entirely different from that exhibited by the previous dipole model [58], where long raft-like clusters are significantly formed and therefore the order parameter monotonically increases from $\lambda \simeq 30$ with magnetic particle-particle interaction strengths [58]. This clearly suggests that the phase of the particle aggregates is significantly different between these two magnetic particle models. The above-mentioned characteristics from $\lambda \simeq 30$ for the present charge model may be explained in the following manner. The rod-like particles forming a thick chain-like cluster tend to incline in directions normal to that of their belonging cluster, after $\lambda \simeq 30$, due to the interactions with the particles belonging to the other clusters and this leads to a lower system energy as a whole. As the magnetic interaction strength is further increased, the particles aggregate to form complex aggregate structures where raft-like and chain-like clusters are combined in a significantly complex formation. At the strength $\lambda = 60$, these complex aggregates are significantly formed and therefore the orientational relationship between particles almost disappears, which gives rise to almost zero value of $S^{(e)} \simeq 0.02$ at $\lambda = 60$. For reference, the result for a strong magnetic field case $\xi = 15$ is also shown in Fig. 3, where it is seen that the dependence of the order parameter on the magnetic interaction strength is quite similar to that for the case of almost no applied magnetic field.

### 7.2. For the case of a strong magnetic field strength

Next, we discuss results for the case of a strong magnetic field strength $\xi = 15$. Fig. 4(a) and (b) show snapshots of the aggregate structures for $\lambda = 20$ and 30, respectively. Fig. 5 shows the dependence of the order parameter on the magnetic field strength for the three cases of the magnetic interaction strength $\lambda = 20$, 30 and 50.

For the case of $\lambda = 20$, shown in Fig. 4(a), the particles strongly tend to incline toward the magnetic field direction because the effect of the magnetic field strength is much larger than the effect of the thermal energy in this situation. From the snapshot on the right-hand side of Fig. 4(a), it is seen that the aggregates are in a wall-like formation but the internal structure does not seem to be sufficiently strong or rigid. That is, these wall-like clusters have a looser internal structure, which is similar to those shown in Fig. 2 (a) for the case of almost no magnetic field. We, therefore, understand that a strong magnetic field induces a change in aggregate structures from loosely-packed into loose wall-like clusters. This regime change in the aggregate structures is evidently reflected by the result of the order parameter shown in Fig. 5. In the range of $\xi \lesssim 10$, the order parameter tends almost zero and then increases steeply from $\lambda \simeq 12$, where a regime change begins and moves towards the above-mentioned wall-like clusters.

For the case of $\lambda = 30$ in Fig. 4(b), the thick chain-like clusters in the magnetic field direction, shown in Fig. 2(b), thicken by adsorbing the neighboring clusters that incline in the opposite direction as the magnetic field strength increases. These thicker clusters are seen to have a tendency to form in the wall-like structure for-

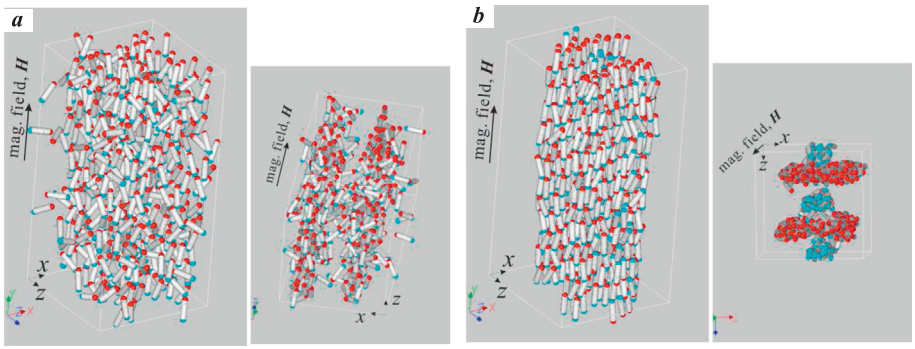


**Fig. 4.** Aggregate structures for the magnetic field strength $\xi = 15$: (a) $\lambda = 20$ and (b) $\lambda = 30$.

mation, which is clearly observed in the snapshot on the right-hand side of Fig. 4(b). By considering these results, we understand that in contrast to the previous dipole model [58], for the present charge model, a significant phase change in the particle aggregates is not induced by an increase in the magnetic field strength. It is noted that raft-like clusters, seen in the dipole model [58], do not appear but the basic clusters are nevertheless the linear and thick chain-like formation found in the present charge model. The order parameter, shown in Fig. 5, is seen to decrease slightly but does not significantly depend on the magnetic field strength, for instance, a value $S^{(e)} \simeq 0.5$ even for $\xi = 20$. This implies that the thick chain-like cluster formation still remains in this range of the external magnetic field for $\lambda = 30$.

For the case of $\lambda = 50$, the curve of the order parameter shown in Fig. 5 exhibits small values such as $S^{(e)} \simeq 0.1$ until $\xi \simeq 13$, and then slightly increases from this magnetic field strength. Although the snapshot is not shown in a figure, we understand that this slight increase is due to the tendency that the particles, which form large aggregates with complex internal structure in the opposite direction to the field direction, start to change their orientation and tend to form thick chain-like clusters that are slightly similar to the snapshot in Fig. 4(b).

## 8. Results and discussion for simple shear flow

### 8.1. Dependence of the aggregate structures on the magnetic field strength

In the present and following section, we discuss results of the aggregate structures using the snapshots and the radial distribution function. We first consider the dependence of the aggregate structures on the magnetic field strength. Fig. 6 shows results of the snapshots of aggregate structures for a weak shear flow $Pe = 1$ and a strong magnetic interaction strength $\lambda = 30$: (a) $\xi = 1$, (b) $\xi = 5$ and (c) $\xi = 20$.

For the case of $\xi = 1$, shown in Fig. 6(a), the cluster formation drastically changes from the linear thick chain-like, shown in Fig. 2(b), into a large complex wall-like structure even at the weak shear flow $Pe = 1$. In the snapshot shown in Fig. 2(b) for thermodynamic equilibrium, thick clusters are formed and the neighboring clusters incline in opposite directions to each other, whereas in the present weak shear flow, short raft-like clusters are formed and these clusters tend to further combine to form a complex wall-like structure. It is seen that this wall-like structure is formed along the shear flow direction in such a way that the plane of the wall is normal to the direction of the angular velocity vector of the shear flow. Moreover, the particles forming raft-like clusters tend to incline toward the shear flow direction even in a weak shear flow. The reason why the thick chain-like clusters inclining in the same and the opposite directions in Fig. 2(b) disappear even in a weak shear flow is that clusters inclining in a direction normal to the shearing plane are substantially influenced by the shear flow and are unable to survive even in the weak shear flow $Pe = 1$. Hence, we understand that in the circumstance of a shear flow and a weak magnetic field, the combination of short raft-like clusters is preferred in the formation of large clusters.

The formation of the short raft-like clusters is verified by the characteristics of the radial distribution function, which are shown in Fig. 7. The curve for $\xi = 1$ in Fig. 7 indicates the radial distribution function has a sharp peak with height $g \simeq 5.5$ at the radial distance $r^* \simeq 1.3$ and approximately a value of two larger than unity in the tail part. The former characteristic with no second or third high peaks implies that short raft-like clusters composed of only two rod-like particles at most are formed in a surface-to-surface contact configuration in the system. The second characteristic suggests that these short clusters are not combined with each other and do not form a larger aggregate by strong cluster-cluster interaction forces, thus the internal structure of the larger aggregates is relatively loose, as clearly observed in Fig. 6(a).

If the magnetic field strength is increased from $\xi = 1$ to $\xi = 5$, shown in Fig. 6(b), and to $\xi = 20$, shown in Fig. 6(c), a regime

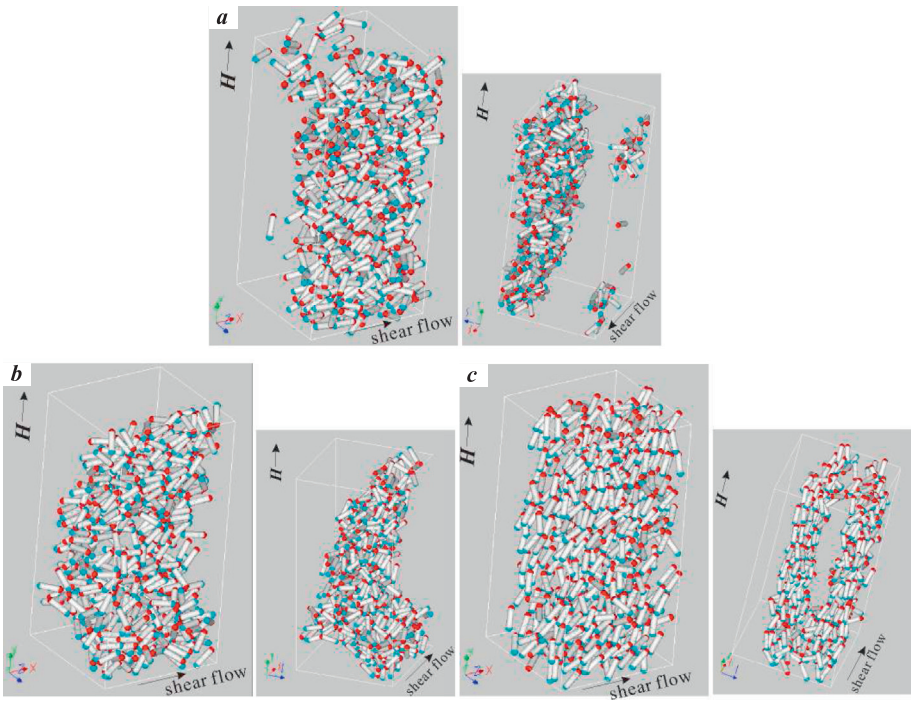


**Fig. 6.** Dependence of the aggregate structures on the magnetic field strength $\xi$ for the case of the magnetic interaction strength $\lambda = 30$ and the Peclet number $Pe = 1$: Fig. 6 (a), (b) and (c) are for $\xi = 1$, 5 and 20, respectively, and the snapshot on the right-hand side of each figure is a different angle view for observing the aggregate structures more clearly.

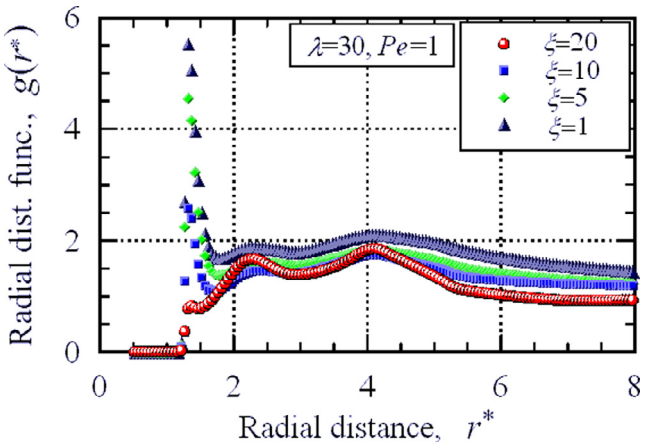


**Fig. 7.** Radial distribution function for the four cases of the magnetic field strength $\xi = 1$, 5, 10 and 20 in the situation of the magnetic interaction strength $\lambda = 30$ and the Peclet number $Pe = 1$.

change arises from a large wall-like aggregate composed of short raft-like clusters into several wall-like structures that are made by an aggregation of thick chain-like clusters, via an intermediary complex aggregate shown in Fig. 6(b). This intermediary aggregate formation is understood to be in the process where raft-like clusters are dissociated and transformed into thick chain-like clusters where the constituent rod-like particles strongly incline in the field direction.

The disappearance of the short raft-like clusters with increasing magnetic field strength is reflected by a characteristic of the radial distribution function, shown in Fig. 7. That is, the first peak becomes lower with magnetic field strength and finally disappears at $\xi = 20$. On the other hand, the peak at $r^* \simeq 4$ comes to appear more clearly, and with increasing radial distance the curve exhibits almost unity in value, significantly lower than those for the other cases. These characteristics evidently show that thick chain-like clusters are formed in the system, but these clusters have relatively loose internal structure, as shown in Fig. 6(c).

We will understand in the following sections that the regime change in clusters from raft-like aggregates into thick chain-like aggregates has a significant effect on the magneto-rheological characteristics of a magnetic rod-like particle suspension.

### 8.2. Dependence of the aggregate structures on the shear rate

We next consider the dependence of the aggregate structures on the shear rate, i.e., the Peclet number. Fig. 8 shows results of the snapshots of aggregate structures for a strong magnetic interaction strength $\lambda = 30$ and a weak magnetic field $\xi = 1$: Fig. 8 (a) and (b) are for $Pe = 5$ and 20, respectively. The snapshot shown in Fig. 6(a) for the case of $Pe = 1$ is referred to for discussion.

As already clarified, for the case of $\xi = 1$, a large wall-like structure is formed by a combination of short raft-like clusters. Since the shear flow is quite weak in this situation, the constituent particles of these short raft-like clusters partially tend to incline in the direction of the angular velocity vector of the shear flow. If the shear rate is increased from $Pe = 1$ to $Pe = 5$, shown in Fig. 8(a), it is seen that the wall-like aggregate is significantly distorted by the shear flow. This is mainly because the shear flow induces an instability of the short raft-like clusters, whose constituent particles incline in the direction of the angular velocity vector. That is, the shear flow functions to make such constituting particles incline in the shear flow direction so that the raft-like clusters is not subject to a large viscous resistance in such a configuration. This suggestion may be verified by the snapshot for the larger shear rate $Pe = 20$, shown in Fig. 8(b). From this snapshot, it is seen that the rod-like particles have a strong tendency to incline along the shear flow direction, and the short raft-like clusters do not disappear but survive even in this strong shear flow situation. As observed in Fig. 8(b), the constituent particles forming a raft-like cluster still incline in the opposite directions to each other, along the shear flow direction; there are only quite few single rod-like particles and constituting particles of short raft-like clusters that incline along the angular velocity vector. After all, a strong shear flow induces a regime change in the internal structure from the compact wall-like aggregate in Fig. 6(a) into the loose aggregate in Fig. 8(b) where the single and short raft-like clusters spread over the whole area of the system and each rod-like particle strongly tends to incline along the shear flow direction. These characteristics of the internal structure of the aggregates may be clearer by considering the results of the radial distribution function.

Fig. 9 shows results of the radial distribution function for a strong interaction strength $\lambda = 30$ and a weak external magnetic field $\xi = 1$ for the four cases of the Peclet number, $Pe = 1$, 5, 10 and 20. You can see that only one significant peak arises at $r^* \simeq 1.3$ for all the cases of the Peclet number, and for the cases except $Pe = 1$, the shape of the tail portion is quite similar to each other and exhibits an almost constant value of unity. On the other hand, the height of the first peak at $r^* \simeq 1.3$ is quite similar among all the cases, and therefore it is almost independent of the shear rate. This implies that the short raft-like clusters do not dissociate due to the influence of the shear flow and remain even in a strong shear flow situation, although the wall-like structure changes in the loose aggregate structure. The reason why the tail part of the radial distribution function shows a value of about two with a weak peak at $r^* \simeq 4.0$ has already been considered in the previous section.

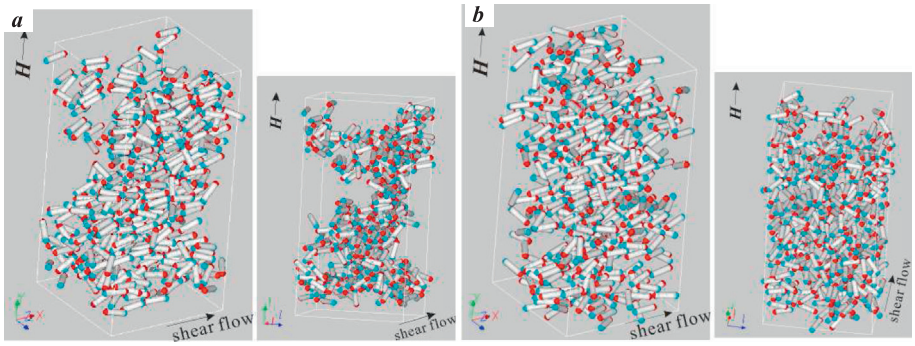


**Fig. 8.** Dependence of the aggregate structures on the Peclet number $Pe$ for the case of the magnetic interaction strength $\lambda = 30$ and the magnetic field strength $\xi = 1$: (a) $Pe = 5$ and (b) $Pe = 20$.

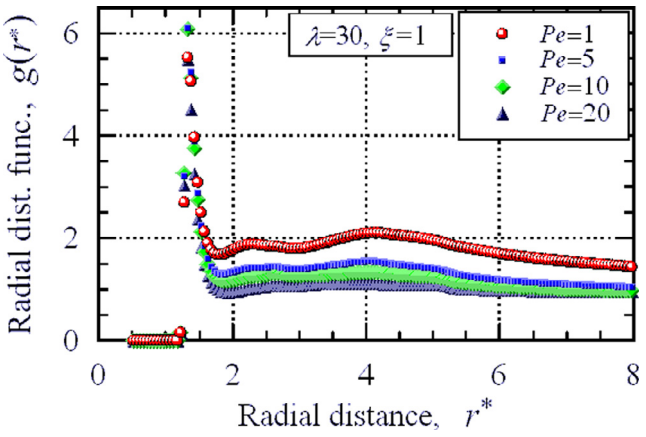


**Fig. 9.** Radial distribution function for the four cases of the Peclet number, $Pe = 1$, 5, 10 and 20 in the case of the magnetic interaction strength $\lambda = 30$ and the magnetic field strength $\xi = 1$.

### 8.3. Dependence of the viscosity on the magnetic particle-particle interaction strength

In this and following sections, we consider the magneto-rheological characteristics of the magnetic rod-like particle suspension by focusing on the net viscosity $\eta_{yx}^{total}$ ($=\eta_{yx}^{M}$), and the three viscosity components $\eta_{yx}^{F}$, $\eta_{yx}^{TH}$ and $\eta_{yx}^{FT}$, which have previously been described. We first address the dependence of the viscosity on the magnetic particle-particle interaction strength. Fig. 10 shows results of the net viscosity and the viscosity components for a weak shear flow $Pe = 1$: Fig. 10(a), (b) and (c) show respectively the net viscosity $\eta_{yx}^{tottal}$, the viscosity component $\eta_{yx}^{TH}$, and in combination the viscosity components $\eta_{yx}^{F}$ and $\eta_{yx}^{FT}$. Each figure has results for the three cases of the magnetic field strength, $\xi = 1$, 10 and 20.

We first consider the results for the net viscosity shown in Fig. 10(a). We can see that the net viscosity monotonically increases with increasing values of the magnetic interaction strength $\lambda$ for all the cases of the magnetic field strength. On the other hand, the curves exhibit qualitative and quantitative differences, which are dependent on the regime of the typical aggregates appearing in the system. In the case of $\xi = 20$, wall-like clusters appear more significantly with increasing magnetic interaction strength from the situation of no cluster formation at $\lambda = 0$. Hence, as clarified below, a simple monotonic increase in the net viscosity is due to the combination of (a) the alignment of the magnetic moment of each particle with the magnetic field direction and (b) the magnetic interactions acting between the constituent particles forming a cluster. For the case of $\xi = 10$, the curve starts to deviate from that for $\xi = 20$ and to increase in a more moderate manner from $\lambda \simeq 20$. These characteristics are mainly due to the appearance of short raft-like clusters in wall-like aggregates, as shown in Fig. 6(a) and (b), in the situation where the magnetic particle-particle interaction is more dominant than the magnetic particle-field interaction. Hence, in the case of $\xi = 1$, this characteristic due to short raft-like clusters in wall-like aggregates start to arise from a small value such as $\lambda \simeq 10$, leading to a curve with a significantly moderate increase because the magnetic particle-particle interaction is much more dominant over the whole range.

We next consider the results of the viscosity component $\eta_{yx}^{TH}$ that is a contribution from the magnetic particle-field interaction. A steep increase in the case of $\xi = 20$ is simply due to the alignment of the magnetic moment of the particles with the magnetic field direction. The wall-like formation without short raft-like clusters enhances this tendency due to the interaction between the constituting rod-like particles, which have already inclined in the field direction to a certain degree due to the particle-field interactions. In the case of $\xi = 10$, short raft-like clusters are formed in wall-like clusters more significantly with increasing magnetic interaction strength, so that the viscosity component does not exhibit a significant increase, in contrast to the previous case of $\xi = 20$. This is quite understandable because the magnetic moments of the neighboring particles in short raft-like clusters align in opposite directions to each other. Therefore, the torques acting on the constituents particles, due to the interaction with the external magnetic field, will cancel to give rise to a small contribution to the viscosity component. The almost zero values for $\xi = 1$ and for any value of $\lambda$ are simply due to significantly weak interactions

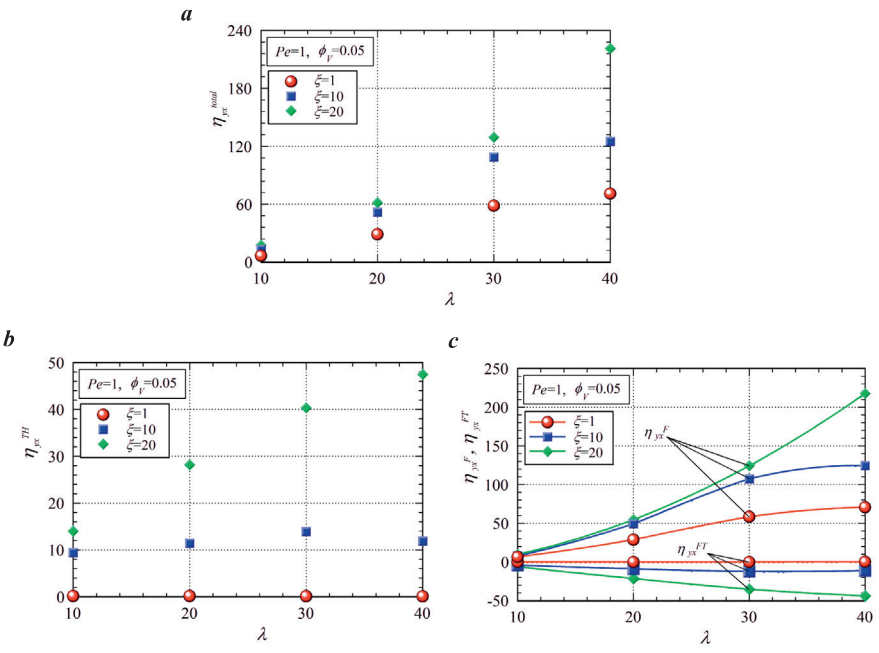


**Fig. 10.** Dependence of the viscosities on the magnetic interaction strength $\lambda$ for $Pe = 1$: (a) the net viscosity $\eta_{vx}^{total}$ ($=\eta_{vx}^{M}$), and the viscosity components (b) $\eta_{VX}^{TH}$ and (c) $\eta_{VX}^{F}$ and $\eta_{VX}^{FT}$.

between the magnetic moment of each particle and the external magnetic field. We will below recognize that in the present situation in regard to the formation of aggregate structures, the contribution from the viscosity component $\eta_{yx}^{TH}$ to the net viscosity is relatively small compared with the contribution of the following viscosity component due to magnetic particle-particle interactions.

We finally consider the results of the viscosity components $\eta_{yx}^{F}$ and $\eta_{yx}^{FT}$, which are the contributions from the forces and the torques, respectively, that arise from the interactions between rod-like particles. We first consider the results of $\eta_{yx}^{F}$ and then those of $\eta_{yx}^{FT}$. From the curves of $\eta_{yx}^{F}$, we can see that the main contribution to the net viscosity is the viscosity component $\eta_{yx}^{F}$, which is straightforwardly recognized by comparing the curves with those shown in Fig. 10(a). This may be reasonable because we are not treating a dilute system but rather a system where aggregate structures are significantly formed throughout and where magnetic particle-particle interactions play an important role in determining the physical characteristics of the magnetic rod-like particle suspension. The shape of the curves is quite similar to that of those of the net viscosity, so that the discussion given above regarding the net viscosity is still valid for explaining the dependence of the viscosity component $\eta_{yx}^{F}$ on the magnetic interaction strength for all the cases of the magnetic field strength. We, therefore, proceed to the discussion regarding the results of the viscosity component $\eta_{yx}^{FT}$. From the result for the case of $\xi = 20$, it is seen that the viscosity becomes negative and monotonically decreases with increasing magnetic interaction strengths. As already pointed out, in this case the particles form a wall-like aggregate without there being short raft-like clusters inside the aggregate, starting from the state of no cluster formation, with increasing magnetic interaction strength. The neighboring rod-like particles forming a cluster naturally tend to incline in the opposite directions to each other as the magnetic particle-particle interaction tends to be dominant. However, the appearance of such a configuration is inhibited by a strong magnetic field such as $\xi = 20$. This inherent tendency in the configuration of neighboring particles functions to accelerate the flow field via the particle-field interaction torques, which leads to the negative values of the viscosity component $\eta_{yx}^{FT}$. The characteristic of the negative viscosity for $\xi = 10$ is much smaller than that for $\xi = 20$. This is due to the tendency that short small clusters can be formed in this intermediary magnetic field strength $\xi = 10$. Hence, since the larger aggregates are mainly composed of short raft-clusters for the significantly weak field strength $\xi = 1$, it is entirely reasonable that the viscosity is independent of the magnetic interaction strength but exhibits almost zero value in the range of $\lambda \lesssim 40$.

### 8.4. Dependence of the viscosity on the magnetic field strength

In this section, we consider the dependence of the magneto-rheological characteristics on the magnetic field strength in a situation of a weak shear flow $Pe = 1$. Fig. 11 shows results of the net viscosity and the viscosity components: Fig. 11(a), (b) and (c) are for the net viscosity $\eta_{yx}^{total}$ ($=\eta_{yx}^{M}$), the viscosity component $\eta_{yx}^{TH}$, and the other viscosity components $\eta_{yx}^{F}$ and $\eta_{yx}^{FT}$, respectively. Each figure has results for the three cases of the magnetic interaction strength, $\lambda = 20$, 30 and 40.

We first discuss the results of the net viscosity shown in Fig. 11 (a). For the case of $\lambda = 40$, the curve monotonically increases until $\xi \simeq 10$, and after that, it starts to increase more steeply, which results from a regime change in the aggregate structures from wall-like structures including short raft-like clusters into larger wall-like aggregates where the constituent rod-like particles tend to incline strongly towards the magnetic field direction. The wall-like aggregates without the shorter raft-like clusters, as shown in Fig. 6(c), inevitably induce a considerable resistance to the ambient flow, which leads to a larger value of the viscosity. Similarly, for the case of $\lambda = 30$, the net viscosity starts to increase more steeply from $\xi \simeq 5$, more moderately from $\xi \simeq 10$ and finally converges to a constant value from $\xi \simeq 15$. These characteristics are quite similar to those for the previous case $\lambda = 40$, but the steeper increase in the net viscosity starts at a lower field strength. This is because the effect of the applied magnetic field on the regime change in the aggregates should become evident at a weaker magnetic field strength for the case of a weaker magnetic interaction strength. The reason why the viscosity converges to a particular value at a threshold field is that where the magnetic moments of all rod-like particles have sufficiently inclined in the magnetic field direction, the internal structure of the larger wall-like aggregates does not substantially change for an increase in field strength

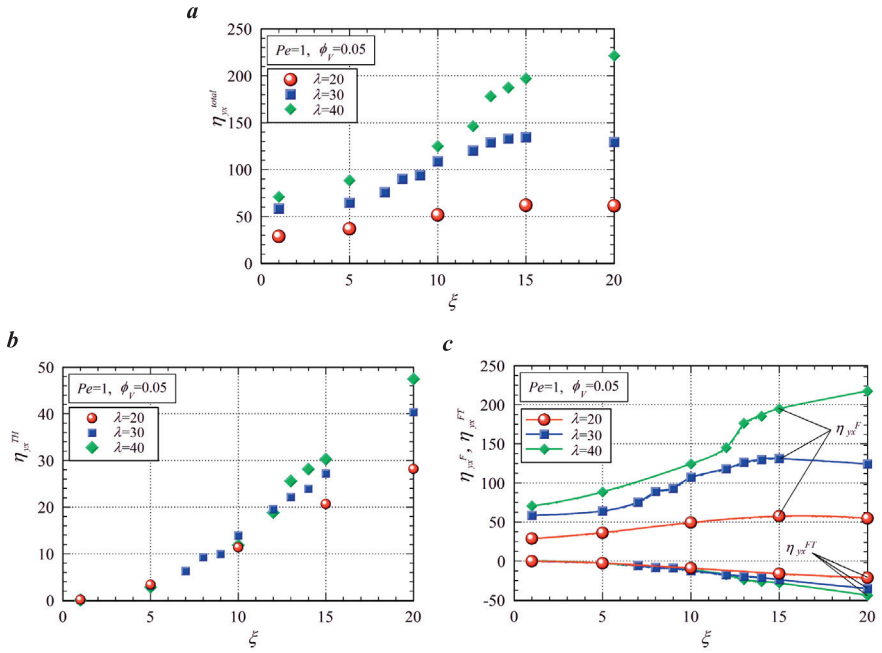


**Fig. 11.** Dependence of the viscosities on the magnetic field strength $\xi$ for $Pe = 1$: (a) the net viscosity $\eta_{vx}^{total}$ ($=\eta_{Vx}^{M}$), and the viscosity components (b) $\eta_{vx}^{TH}$ and (c) $\eta_{Vx}^{F}$ and $\eta_{Vx}^{FT}$.

and gives rise to an almost constant value of the net viscosity, as shown in the curve for $\lambda = 30$ in Fig. 11(a). For the case of $\lambda = 20$, the curve monotonically increases in a moderate manner and converges to a certain value from $\xi = 15$. In this case, a regime change in the aggregates does not arise from a change in the field strength, so the behaviour of the net viscosity seems to be quite reasonable. Similar to the previous result shown in Fig. 10(a), the contribution of the viscosity component $\eta^F_{yx}$ to the net viscosity is a consequence of the volumetric fraction, which will be recognized below.

We now consider the results of the viscosity component $\eta^{TH}_{yx}$, shown in Fig. 11(b). It is seen that the viscosity gradually increases from zero and exhibits an almost linear increase from a certain field strength. This dependence of the viscosity on the magnetic field strength is common among the three cases, but the threshold field strength from which a linear increase starts is dependent on the value of the magnetic interaction strength. All three curves increase with field strength, the curve for $\lambda = 20$ first starts to deviate from the other curves at $\xi \simeq 5$, then the curve for $\lambda = 30$ deviates from that for $\lambda = 40$ at $\xi \simeq 10$, after which each curve increases in a linear manner. These threshold field strengths correspond to those for the start of the larger increases observed in Fig. 11 (a). The linear increase from each threshold field strength is due to the contribution of the alignment of the magnetic moments with the magnetic field where there is no appearance of a regime change in the aggregate structures; a larger interaction between the particle and the applied magnetic field gives rise to a larger value of the viscosity component $\eta^{TH}_{yx}$.

Finally, we briefly consider the results of the viscosity components $\eta^F_{yx}$ and $\eta^{FT}_{yx}$, shown in Fig. 11(c). By comparing the present result with that in Fig. 11(a), we can straightforwardly understand that the viscosity component $\eta^F_{yx}$ is the main contribution to the net viscosity; all three curves are in good agreement with the corresponding curves of Fig. 11(a) and (c) in both their qualitative and quantitative meaning. Hence, the mechanism for the steep increase from $\xi \simeq 10$ for $\lambda = 40$ and from $\xi \simeq 5$ for $\lambda = 30$ is similar to the curves of the net viscosity in Fig. 11(a). As explained above, the reason why the viscosity component $\eta^{FT}_{yx}$ becomes negative and decreases with increasing magnetic field strength is due to the inherent tendency regarding neighboring particles forming a cluster in a configuration where they naturally tend to incline in the opposite directions to each other. This configuration gives rise to a stability in the cluster under the conditions of the magnetic interaction being dominant compared with the external magnetic field.

### 8.5. Dependence of the viscosity on the shear rate

Finally, we discuss the dependence of the magneto-rheological effect on the shear rate. Fig. 12 shows the dependence of the net viscosity on the Peclet number that corresponds to the shear rate, for the three cases of the magnetic field strength $\xi = 1$, 10 and 20. Since the dependence on the Peclet number of all the viscosity components is quite similar to that of the net viscosity, we here focus only on the characteristics of the net viscosity. It is seen from Fig. 12 that the viscosity significantly decreases in a monotonic manner within the range of $Pe \lesssim 10$, and in the region of $Pe \gtrsim 10$ it tends to zero. As previously understood from the results shown in Figs. 8 and 9, the simple shear flow does not induce a drastic regime change in the aggregate structures, in particular, the wall-like aggregates, both with or without small raft-like clusters, do not substantially change for an increase in the Peclet number. Hence, an increase in the shear rate will function to simply decrease the effect of the magnetic particle-particle and the particle-field interactions. This leads to a monotonic reduction in the net viscosity and all the viscosity components, and they exhibit small values in the range where the shear flow is more dominant than the magnetic interaction and the external magnetic field.

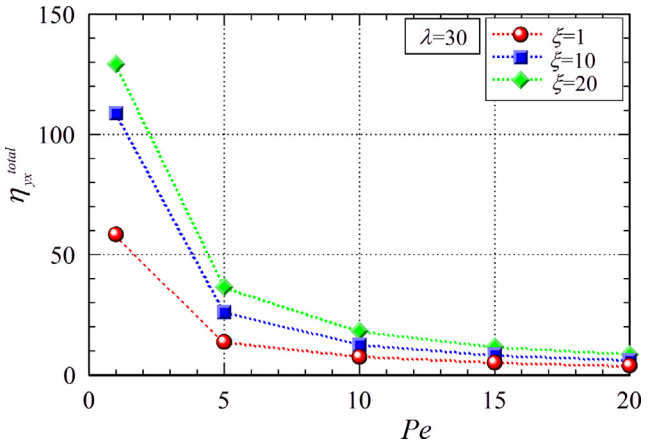


**Fig. 12.** Dependence of the net viscosity on the Peclet number for the strong magnetic interaction strength $\lambda = 30$, where the results are shown for the three cases of the magnetic field strength, $\xi = 1$, 10 and 20.

## 9. Conclusion

In the present study, we have addressed a suspension composed ferromagnetic rod-like particles that are modelled as a spherocylinder with a plus and a minus magnetic charge at the centre of each hemisphere cap. Monte Carlo simulations have been employed for investigating the aggregate structures of the rod-like particles in a thermodynamic equilibrium situation, i.e. with no shear flow. Brownian dynamics simulations have been employed for elucidating magneto-rheological characteristics of the suspension in a simple shear flow. From the former simulations, we have clarified the dependence of the regime change in the aggregate structures on the magnetic field strength and the magnetic particle-particle interaction strength. From the latter simulations, we have clarified the dependence of the aggregate structures and the magneto-rheological characteristics on the above-mentioned factors and the shear flow. In order to investigate the magneto-rheological effect in more detail, we have addressed the three viscosity components which arise from the torque due to the magnetic particle-field interaction and the torque and the force due to the magnetic interactions between the particles. The results obtained in the present study are summarized as follows. For the case of thermodynamic equilibrium, without a shear flow and no applied magnetic field, if the magnetic particle-particle interaction is sufficiently strong the rod-like particles aggregate to form thick chain-like clusters, and the neighboring clusters incline in opposite directions. In an increasing external magnetic field, the thick chain-like clusters in the magnetic field direction grow thicker by adsorbing the neighboring clusters that incline in the opposite direction. These thicker clusters are seen to have a tendency to be formed in a wall-like structure formation. Hence, for the present charge model, a significant phase change in the particle aggregates is not induced by an increase in the magnetic field strength. For the case of a simple shear flow, even a weak shear flow induces a significant regime change from the thick chain-like clusters of thermodynamic equilibrium into the wall-like aggregates composed of short raft-like clusters of the shear flow case. A strong external magnetic field drastically changes these aggregates into wall-like aggregates that are composed of thick chain-like clusters rather than the short raft-like clusters. Although a strong shear flow significantly inclines the constituent rod-like particles toward the magnetic field direction, the internal structure of these aggregates is not strongly influenced by a shear flow, and the formation of raft-like clusters is still maintained inside the aggregates. The main contribution to the net viscosity is the

viscosity component due to magnetic particle-particle interaction forces, which may be reasonable because we do not treat a significantly dilute situation but a situation where aggregate structures are significantly formed in the whole system. Hence, a larger magnetic interaction and also a stronger external magnetic field give rise to a larger magneto-rheological effect. However, the dependence of the viscosity on these factors is governed in a complex manner by whether or not a wall-like aggregate is composed mainly of short raft-like clusters. Linear chain-like clusters, which are formed by the positive and the negative charges of neighboring particles tending to be in contact, give rise to a larger flow resistance and thus a larger magneto-rheological effect. Since a simple shear flow does not induce a drastic regime change in the aggregate structures, an increase in the shear rate functions to simply decrease the effect of the magnetic particle-particle and particle-field interactions leading to a monotonic decrease in the net viscosity and corresponding viscosity components.

## References


[1] R.E. Rosensweig, Ferrohydrodynamics, Cambridge University Press, Cambridge, 1985.
[2] W.A. Bullough (Ed.), Electro-Rheological Fluids, Magneto-Rheological Suspensions and Associated Technology, World Scientific, Singapore, 1996.
[3] N.M. Wereley (Ed.), Magnetorheology: Advances and Applications, Royal Society of Chemistry, London, 2013.
[4] F. Jorgensen, The Complete Handbook of Magnetic Recording, 4th ed., McGraw-Hill, New York, 1996.
[5] U. Häfeli, W. Schütt, J. Teller, M. Zborowski (Eds.), Scientific and Clinical Applications of Magnetic Carriers, Springer, Berlin, 1997.
[6] C.E. Alvarez, S.H.L. Klapp, Translational and rotational dynamics in suspensions of magnetic nanorods, Soft Matter 9 (2013) 8761–8770.
[7] J.H. Sanchez, C. Rinaldi, Rotational Brownian dynamics simulations of non-interacting magnetized ellipsoidal particles in d.c. and a.c. magnetic fields, J. Magn. Magn. Mater. 321 (2009) 2985–2991.
[8] A. Gil-Villegas, G. Jackson, S.C. McGrother, Computer simulation of dipolar liquid crystals, J. Mol. Liquids. 76 (1998) 171–181.
[9] D. Horák, M. Babič, H. Macková, M.J. Beneš, Preparation and properties of magnetic nano- and microsized particles for biological and environmental separations, J. Separation Sci. 30 (2007) 1751–1772.
[10] J. De Vicente, J.P. Segovia-Gutiérrez, E. Andablo-Reyes, F. Vereda, R. Hidalgo-Álvarez, Dynamic rheology of sphere- and rod-based magnetorheological fluids, J. Chem. Phys. 131 (2009) 194902.
[11] S. Chikazumi, Physics of Ferromagnetism, 2nd ed., Oxford Science Publications, London, 1997.
[12] P. Kuzhir, C. Magnet, G. Bossis, A. Meunier, V. Bashtovoi, Rotational diffusion may govern the rheology of magnetic suspensions, J. Rheology. 55 (2011) 1297–1318.
[13] S. Dussi, L. Rovigatti, F. Sciortino, On the gas–liquid phase separation and the self-assembly of charged soft dumbbells, Molec. Phys. 111 (2013) 3608–3617.
[14] D.C. Williamson, N.A. Thacker, S.R. Williams, Effects of intramolecular dipolar coupling on the isotropic-nematic phase transition of a hard spherocylinder fluid, Phys. Rev. E. 71 (2005) 021702.
[15] B.W. Kwaadgras, R. Van Roij, M. Dijkstra, Self-consistent electric field-induced dipole interaction of colloidal spheres, cubes, rods, and dumbbells, J. Chem. Phys. 140 (2014) 154901.
[16] C.E. Alvarez, S.H.L. Klapp, Percolation and orientational ordering in systems of magnetic nanorods, Soft Matter 8 (2012) 7480–7489.
[17] P.I. Girginova, A.L. Daniel-da-Silva, C.B. Lopes, P. Figueira, M. Otero, V.S. Amaral, E. Pereira, T. Trindade, Silica coated magnetite particles for magnetic removal of Hg2+ from water, J. Colloid Interface Sci. 345 (2010) 234–240.
[18] S. Lan, X. Wu, L. Li, M. Li, F. Guo, S. Gan, Synthesis and characterization of hyaluronic acid-supported magnetic microspheres for copper ions removal, Colloids Surf. A 425 (2013) 42–50.
[19] I.J. Bruce, T. Sen, Surface modification of magnetic nanoparticles with alkoxysilanes and their application in magnetic bioseparations, Langmuir 21 (2005) 7029–7035.
[20] F. Selimefendigil, H.F. Öztop, K. Al-Salem, Natural convection of ferrofluids in partially heated square enclosures, J. Magn. Magn. Mater. 372 (2014) 122–133.
[21] F. Selimefendigil, H.F. Öztop, Forced convection of ferrofluids in a vented cavity with a rotating cylinder, Int. J. Therm. Sci. 86 (2014) 258–275.
[22] F. Selimefendigil, H.F. Öztop, A.J. Chamkha, MHD mixed convection and entropy generation of nanofluid filled lid driven cavity under the influence of inclined magnetic field, J. Magn. Magn. Mater. 406 (2016) 266–281.
[23] F. Selimefendigil, H.F. Öztop, Analysis of MHD mixed convection in a flexible walled and nanofluids filled lid-driven cavity with volumetric heat generation, Int. J. Mech. Sci. 118 (2016) 113–124.
[24] F. Selimefendigil, H.F. Öztop, Natural convection in a flexible sided triangular cavity with internal heat generation under the effect of inclined magnetic field, J. Magn. Magn. Mater. 417 (2016) 327–337.
[25] F. Selimefendigil, H.F. Öztop, MHD mixed convection and entropy generation of power law fluids in a cavity with a partial heater under the effect of a rotating, Int. J. Heat Mass Transfer 98 (2016) 40–51.
[26] A.A. Kuznetsov, V.I. Filippov, O.A. Kuznetsov, V.G. Gerlivanov, E.K. Dobrinsky, S. I. Malashin, New ferro-carbon adsorbents for magnetically guided transport of anti-cancer drugs, J. Magn. Magn. Mater. 194 (1999) 22–30.
[27] J. Weingart, P. Vabbilisetty, X. Sun, Membrane mimetic surface functionalization of nanoparticles: Methods and applications, Advan. Colloid Interface Sci. 197–198 (2013) 68–84.
[28] A.M. Schmidt, Thermoresponsive magnetic colloids, Colloid Polym. Sci. 285 (2007) 953–966.
[29] Q.A. Pankhurst, J. Connolly, S.K. Jones, J. Dobson, Applications of magnetic nanoparticles in biomedicine, J. Phys. D: Appl. Phys. 36 (2003) R167.
[30] I.M. Obaidat, B. Issa, Y. Haik, Magnetic properties of magnetic nanoparticles for efficient hyperthermia, Nanomater. 5 (2015) 63–89.
[31] R.E. Rosensweig, Heating magnetic fluid with alternating magnetic field, J. Magn. Magn. Mater. 252 (2002) 370–374.
[32] K. Raj, R. Moskowitz, Commercial applications of ferrofluids, J. Magn. Magn. Mater. 85 (1990) 233–245.
[33] K. Raj, B. Moskowitz, R. Casciari, Advances in ferrofluid technology, J. Magn. Magn. Mater. 149 (1995) 174–180.
[34] N. Hasegawa, H. Yoshioka, H. Shingo, Noncontact gravity compensator with magnetic fluid seals, J. Adv. Mech. Des. Syst. Manuf. 10 (2016), p. JAMDSM0078.
[35] C. Holm, J.J. Weis, The structure of ferrofluids: A status report, Curr. Opin. Colloid Interface Sci. 10 (2005) 133–140.
[36] A. Satoh, Rheological properties and particle behaviors of a non-dilute colloidal distribution composed of ferromagnetic spherocylinder particles subjected to a simple shear flow (Analysis by means of mean field approximation), J. Colloid Interface Sci. 262 (2003) 263–273.
[37] T.M. Kwon, P. Frattini, L.N. Sadani, M.S. Jhon, Rheo-optical study of magnetic particle orientation under external fields, Colloids Surf. A 80 (1993) 47–61.
[38] A. Satoh, Influences of magnetic interactions between clusters on particle orientational characteristics and viscosity of a colloidal dispersion composed of ferromagnetic spherocylinder particles: analysis by means of mean field approximation for a simple shear flow, J. Colloid Interface Sci. 289 (2005) 276–285.
[39] E. Cisternas, E.E. Vogel, Inscription and stabilization of ferromagnetic patterns on arrays of magnetic nanocylinders, J. Magn. Magn. Mater. 337 (2013) 74–78.
[40] K. Slyusarenko, D. Constantin, P. Davidson, A two-dimensional nematic phase of magnetic nanorods, J. Chem. Phys. 140 (2014) 104904.
[41] E. Matijevic, P. Scheiner, Ferric hydrous oxide sols: III. Preparation of uniform particles by hydrolysis of Fe(III)-chloride, -nitrate, and -perchlorate solutions, J. Colloid Interface Sci. 63 (1978) 509–524.
[42] M. Ozaki, S. Kratohvil, E. Matijevic, Formation of monodispersed spindle-type hematite particles, J. Colloid Interface Sci. 102 (1984) 146–151.
[43] T.P. Raming, A.J.A. Winnubst, C.M. Van Kats, A.P. Philipse, The synthesis and magnetic properties of nanosized hematite ($\alpha$-Fe2O3) particles, J. Colloid Interface Sci. 249 (2002) 346–350.
[44] M. Ozaki, N. Ookoshi, E. Matijević, Preparation and magnetic properties of uniform hematite platelets, J. Colloid Interface Sci. 137 (1990) 546–549.
[45] D. Van der Beek, H. Reich, P. Van der Schoot, M. Dijkstra, T. Schilling, R. Vink, M. Schmidt, R. Van Roij, H. Lekkerkerker, Isotropic-nematic interface and wetting in suspensions of colloidal platelets, Phys. Rev. Lett. 97 (2006) 087801.
[46] G. Cheng, R.D. Shull, A.R.H. Walker, Dipolar chains formed by chemically synthesized cobalt nanocubes, J. Magn. Magn. Mater. 321 (2009) 1351–1355 (H03).
[47] M. Aoshima, M. Ozaki, A. Satoh, Structural analysis of self-assembled lattice structures composed of cubic hematite particles, J. Phys. Chem. C 116 (2012) 17862–17871.
[48] S.I.R. Castillo, C.E. Pompe, J. Van Mourik, D.M.A. Verbart, D.M.E. Thies-Weesie, P.E. De Jongh, A.P. Philipse, Colloidal cubes for the enhanced degradation of organic dyes, J. Mater. Chem. A 2 (2014) 10193–10201.
[49] J.M. Meijer, D. Byelov, L. Rossi, A. Snigirev, I. Snigireva, A.P. Philipse, A.V. Petukhov, Self-assembly of colloidal hematite cubes: a microradian X-ray diffraction of exploration of sedimentary crystals, Soft Matter 9 (2013) 10729–10738.
[50] M.V. Kovalenko, M.I. Bodnarchuk, R.T. Lechner, G. Hesser, F. Schäffler, W. Heiss, Fatty acid salts as stabilizers in size- and shape-controlled nanocrystal synthesis: the case of inverse spinel iron oxide, J. Am. Chem. Soc. 129 (2007) 6352–6353.
[51] E. Wetterskog, M. Agthe, A. Mayence, J. Grins, D. Wang, S. Rana, A. Ahniyaz, G. Salazar-Alvarez, L. Bergström, Precise control over shape and size of iron oxide nanocrystals suitable for assembly into ordered particle arrays, Sci. Technol. Adv. Mater 15 (2014) 055010.
[52] R.M. Erb, H.S. Son, B. Samanta, V.M. Rotello, B.B. Yellen, Magnetic assembly of colloidal superstructures with multipole symmetry, Nature Lett. 457 (2009) 999–1002.
[53] C. Hellenthal, W. Ahmed, E.S. Kooij, A. Van Silfhout, B. Poelsema, H.J.W. Zandvliet, Tuning the dipole-directed assembly of core-shell nickel-coated gold nanorods, J. Nanopart. Res. 14 (2012) 1–14.
[54] S. Heidenreich, S. Hess, S.H.L. Klapp, Shear-induced dynamic polarization and mesoscopic structure in suspensions of polar nanorods, Phys. Rev. Lett. 102 (2009) 028301.

[55] J.H. Sánchez, C. Rinaldi, Magnetoviscosity of dilute suspensions of magnetic ellipsoids obtained through rotational Brownian dynamics simulations, J. Colloid Interface Sci. 331 (2009) 500–506.
[56] P. Kuzhir, M.T. López-López, G. Bossis, Magnetorheology of fiber suspensions. II. Theory, J. Rheol. 53 (1) (2008) 127.
[57] P. Kuzhir, C. Magnet, L. Rodriguez Arco, M. Lopez-Lopez, H. Fezai, A. Meunier, A. Zubarev, G. Bossis, Magnetorheological effect in the magnetic field oriented along the vorticity, J. Rheol. 58 (2014) 1829.
[58] A. Satoh, Monte Carlo simulations on phase change in aggregate structures of ferromagnetic spherocylinder particles, Colloids Surf. A 504 (2016) 393–399.
[59] H.J. Choi, C.A. Kim, T.M. Kwon, M.S. John, Viscosity of magnetic particle suspensions, J. Magn. Magn. Mater. 209 (2000) 228–230.
[60] R.C. Bell, E.D. Miller, J.O. Karli, A.N. Vavreck, D.T. Zimmerman, Influence of particle shape on the properties of magnetorheological fluids, Inter. J. Modern Phys. B 21 (2007) 5018–5025.
[61] J. de Vicente, F. Vereda, J.P. Segovia-Gutiérrez, R. Hidalgo-Álvarez, Effect of particle shape in magnetorheology, J. Rheology 54 (2010) 1337–1343.
[62] A.R. Altenberger, J.S. Dahler, Theoretical rheology of suspensions of ferromagnetic rod-like particles, Int. J. Thermophys. 10 (1989) 183–197.
[63] A. Satoh, Rheological properties and orientational distributions of dilute ferromagnetic spherocylinder particle dispersions (Approximate solutions by means of Galerkin's method), J. Colloid Interface Sci. 234 (2001) 425–433.
[64] M. Ozaki, E. Matijević, Preparation and magnetic properties of monodispersed spindle-type $\gamma$-$Fe_2O_3$ particles, J. Colloid Interface Sci. 107 (1985) 199.
[65] L.C. Varanda, M. Jafelicci Jr., G.F. Goya, Magnetic properties of spindle-type iron fine particles obtained from hematite, J. Magn. Magn. Mater. 226–230 (2001) 1933.
[66] A. Satoh, M. Ozaki, Transport coefficients and orientational distributions of spheroidal particles with magnetic moment normal to the particle axis: Analysis for an applied magnetic field normal to the shear plane, J. Colloid Interface Sci. 298 (2006) 957.
[67] A. Satoh, Y. Sakuda, Negative viscosity due to magnetic properties of a non-dilute suspension composed of ferromagnetic rod-like particles with magnetic moment normal to the particle axis, Mol. Phys. 105 (2007) 3145.
[68] A. Satoh, Influence of the spin Brownian motion on the negative magneto-rheological effect in a rod-like hematite particle suspension, Mol. Phys. 111 (2013) 1042–1052.
[69] A. Satoh, Brownian dynamics simulations with spin Brownian motion on the negative magneto-rheological effect of a rod-like hematite particle suspension, Mol. Phys. 113 (2015) 656–670.
[70] Y. Sakuda, M. Aoshima, A. Satoh, Negative magneto-rheological effect of a dispersion composed of spindle-like hematite particles, Mol. Phys. 110 (2012) 1429–1435.
[71] A. Satoh, On aggregate structures in a rod-like hematite particle suspension by means of Brownian dynamics simulations, Mol. Phys. 112 (2014) 2122–2137.
[72] D. van der Beek, A.V. Petukhov, P. Davidson, J. Ferré, J.P. Jamet, H.H. Wensink, G.J. Vroege, W. Bras, H.N.W. Lekkerkerker, Magnetic-field-induced orientational order in the isotropic phase of hard colloidal platelets, Phys. Rev. E 73 (2006) 041402.
[73] A. Satoh, Brownian dynamics simulation of a dispersion composed of disk-like hematite particles regarding aggregation phenomena, Colloids Surf. A 483 (2015) 328–340.
[74] A. Satoh, H. Yokoyama, On the behavior of an oblate spheroidal hematite particle in a simple shear flow under a uniform magnetic field applied in the flow direction, Colloid Polym. Sci. 292 (2014) 935–944.
[75] R.K. Mallavajula, L.A. Archer, D.L. Koch, The average stress in a suspension of cube-shaped magnetic particles subject to shear and magnetic fields, Phys. Fluids 27 (2015) 093101.
[76] A. Satoh, Brownian dynamics simulation of a dispersion composed of disk-like hematite particles regarding the orientational distribution and the magneto-rheological properties, Colloids Surf. A 483 (2015) 341–351.
[77] H. Reich, M. Schmidt, Sedimentation equilibrium of colloidal platelets in an aligning magnetic field, J. Chem. Phys. 132 (2010) 144509.
[78] P. Linse, Quasi-2D fluids of dipolar superballs in an external field, Soft Matter 11 (2015) 3900–3912.
[79] J.G. Donaldson, E.S. Pyanzina, E.V. Novak, S.S. Kantorovicha, Anisometric and anisotropic magnetic colloids: How to tune the response, J. Magn. Magn. Mater. 383 (2015) 267–271.
[80] L. Rossi, V. Soni, D.J. Ashton, D.J. Pine, A.P. Philipse, P.M. Chaikin, M. Dijkstra, S. Sacanna, W.T.M. Irvine, Shape-sensitive crystallization in colloidal superball fluids, U.S.A. (edited by D.A. Weitz), Proc. Natl. Acad. Sci. 112 (2015) 5286–5290.
[81] J.M. Meijer, F. Hagemans, L. Rossi, D. Byelov, S.I.R. Castillo, I. Snigireva, A.P. Philipse, A.V. Petukhov, Self-assembly of colloidal cubes via vertical deposition, Langmuir 28 (2012) 7631–7638.
[82] L. Rossi, S. Sacanna, W.T.M. Irvine, P.M. Chaikin, D.J. Pine, A.P. Philipse, Cubic crystals from cubic colloids, Soft Matter 7 (2011) 4139–4142.
[83] R.K. Mallavajula, D.L. Koch, L.A. Archer, Intrinsic viscosity of a suspension of cubes, Phys. Rev. E. 88 (2013) 052302.
[84] A. Satoh, Introduction to Practice of Molecular Simulation: Molecular Dynamics, Monte Carlo, Brownian Dynamics, Lattice Boltzmann and Dissipative Particle Dynamics, Elsevier Insights, Amsterdam, 2010, pp. 5–19.
[85] A. Satoh, Introduction to Molecular-Microsimulation of Colloidal Dispersions, Elsevier, Amsterdam, 2003.
[86] M.P. Allen, D.J. Tildesley, Computer Simulation of Liquids, Clarendon Press, Oxford, 1987.
[87] A. Satoh, A new technique for Metropolis Monte Carlo simulation to capture aggregate structures of fine particles: Cluster-moving Monte Carlo algorithm, J. Colloid Interface Sci. 150 (1992) 461–472.